Journal of Materials Science: Materials in Electronics (2020) 31:15372–15380
https://doi.org/10.1007/s10854-020-04101-3

# Graphene-based field-effect transistors integrated with microfluidic chip for real-time pH monitoring of seawater

Jianwei Gao[1] · Yanhao Wang[1] · Yingkuan Han[1,2] · Yakun Gao[1] · Chao Wang[1] · Lin Han[1] · Yu Zhang[1]

Received: 30 April 2020 / Accepted: 25 July 2020 / Published online: 3 August 2020
© Springer Science+Business Media, LLC, part of Springer Nature 2020

## Abstract

Seawater pH is an important parameter in marine and environmental researches, and it demands sensitive, portable, rapid and real-time sensing pH sensors. Here, we propose a graphene field-effect transistor (Gr-FET)-based pH sensor on flexible polyimide (PI) substrate integrated with microfluidic chip for real-time seawater pH detection. The monolayer graphene was grown by chemical vapor deposition, and transferred onto PI substrate to form transistor. The formed Gr-FET integrated with microfluidic channel forming the pH sensing chip, which is $2 \times 3$ cm$^2$ in size, and 2 mm in thickness. Gr-FET-based pH sensor on PI substrate presents sensitivity of 23.98 mV/pH and 8.07 mV/pH in $1 \times$PBS and seawater solutions, respectively, and realizes pH detection in 1 min. The different ion type and concentration in the seawater solution could be contributed to the sensitivity reduction of the sensors in seawater. Real-time pH detection results of local fresh seawater show the fluctuation within 3% comparison with commercial pH sensor. The proposed Gr-FET-based pH sensor is economic, portable, fast and promising to realize real-time pH detection.

## 1 Introduction

Graphene is a two-dimensional carbon nanomaterial composed of a carbon atom and a sp$^2$ hybrid orbital to form a hexagonal honeycomb lattice [1–3]. It has excellent optical, electrical and mechanical properties and presents promising application prospects in micro-nano devices, energy, biomedicine and drug delivery [4–6]. Moreover, due to its two-dimensional properties, graphene has excellent conductivity mobility and low noise characteristics as well as good flexibility and ductility, which make it have broad prospects in electrochemical and biological signal detection [7–9]. Graphene grown by chemical vapor deposition (CVD) possesses the attractive advantage of enabling integration in large area and flexible substrates [10–12]. Due to the zero bandgap characteristics of graphene, Gr-FETs have a unique bipolarity [13]. The position of the minimum conductivity point in the transfer characteristic curve of Gr-FET is called the Dirac point. When the surface properties of graphene change, the position of the Dirac point changes [14–16]. Based on this property, many substances such as ions, proteins, DNA and pH can be detected [17–20].

Although paper test strips and glass electrodes are mostly used for pH sensors [21, 22], many studies have focused on developing less fragile, miniaturized and biocompatible sensors with higher sensitivity [23], for instance, Organic

**Electronic supplementary material** The online version of this article (https://doi.org/10.1007/s10854-020-04101-3) contains supplementary material, which is available to authorized users.

✉ Yu Zhang
yuzhang@sdu.edu.cn

Jianwei Gao
gaoxiii@foxmail.com

Yanhao Wang
wangyanhaooo@126.com

Yingkuan Han
yingkuan.han@foxmail.com

Yakun Gao
17854262215@163.com

Chao Wang
980606701@qq.com

Lin Han
hanlin@sdu.edu.cn

[1] Institute of Marine Science and Technology, Shandong University, Qingdao 266237, China

[2] School of Microelectronics, Shandong University, Jinan 250010, China

Field-Effect Transistor [24], nanowire FET pH sensor [25] and graphene-based FET pH sensors [22]. Graphene-based field-effect transistor pH sensors are currently the promising alternative to glass electrodes. Sensitivity is one of the most important parameters during pH sensing, and researchers have investigated several approaches to improve the sensitivity of graphene-based pH sensors [26, 27]. Monolayer Gr-FET on 6H-SiC single crystal was used to improve pH sensitivity, since SiC provided an appropriate interface condition for Gr-FET to sense pH [28]**.** Electron-beam lithography (EBL) and oxygen plasma were used to pattern nanoscale graphene and form FET pH sensor, which improved the sensitivity from 6.5 to 23.6 mV/pH [29]. Patterned nanoscale graphene created some defects at the engineered edges, and appropriate defect density is important for pH sensing performance [30]. Surface functionalization of graphene-based FETs is another approach to improve the Gr-based FET pH sensor sensitivity [26, 31]. In addition, stability is another important parameter of pH sensing. In order to improve the stability of Gr-based FET pH sensor, atomic layer deposited (ALD) aluminum oxide ($Al_2O_3$) and hexagonal boron nitride (h-BN) stacks on graphene were reported recently [32–34]. With those technologies, the properties of Gr-based FET pH sensor could be greatly improved. Some applications were reported based on Gr-based FET pH sensors for chemical [35] and biological [36] sensing [37]. Researchers found that the performance of pH sensor is also related to the composition and ion concentration of test sample [38, 39].

pH of seawater is an important parameter in marine research, which has an important impact on the growth of marine organisms and the stability of marine ecosystem. In recent years, a range of technologies have been developed for seawater pH measurements [23, 27, 40, 41]. These include ion sensitive field-effect transistors (ISFETs) [42], optical pH sensor materials [33] and colorimetry [43]. ISFET-based pH sensors show a slow response because of their thick passivation layers. The production of optical pH sensor materials is complicated. The operation of colorimetry is troublesome and time consuming. As a result, tractable and economic approaches are desired to develop the sensitive Gr-FET-based pH sensor for seawater real-time monitoring. The PBS solution was usually used for pH sensors testing in lab experiments. The pH detection of seawater is different from usual PBS used in laboratory. To the best of our knowledge, the report about seawater pH monitoring using Gr-FET-based pH sensor is lacking.

Here, we report a sensitive, stable and rapid Gr-FET-based pH sensor for real-time seawater pH monitoring, which employed monolayer graphene to form FET on flexible PI substrate with solution gate enabled by integration of microfluidic chip. The sensor on PI substrate presents sensitivity of 23.98 mV/pH and 8.07 mV/pH in 1 × PBS and seawater solutions, and detection time within 1 min. The performance of pH sensor shows stable sensing with cyclic testing and seven days continuous tests of seawater. The microfluidic chip-integrated Gr-FET pH sensor is fast, sensitive, stable and flexible, which has potential applications in real-time pH monitoring of seawater.

## 2 Experimental procedure

Graphene films were grown by atmospheric-pressure CVD on 25 μm copper foils (99.8% purity) using a protocol that has been described in detail elsewhere [44]. Briefly, copper foil was placed in a tube furnace and heated at 1070 °C under a flow of 300 sccm hydrogen for 50 min to remove the native oxide of copper. Then a mixture of 5 sccm methane and 700 sccm hydrogen was introduced into the quartz tube to grow graphene for 30 min. Subsequently, the quartz tube was removed from the heating region of the furnace so that the copper foil was rapidly cooled for monolayer graphene formation [30].

After the graphene growth, the copper foil with monolayer graphene was coated with a protective layer of polymethyl-methacrylate (PMMA) and then copper foil was removed by immersion in a copper etchant (0.1 M ferric chloride solution). Then graphene film with PMMA protective layer was transferred to $20 \times 30$ mm$^2$ $Si/SiO_2$ and PI substrates, and then the samples were immersed in acetone solution for 90 min to remove the PMMA layer. The Raman spectra were tested by Micro Raman spectrometer (Renishaw, UK). 532 nm laser excitation is used with laser power of 1.5 mW, and exposure time is 10 s. Metal electrodes (Ti/Au, 10 nm/50 nm) were evaporated by E-beam Evaporation System to form source/drain contacts of Gr-FET. The size (length and width) of source–drain electrodes is 8 mm × 1 mm. The distance between source and drain electrodes (the channel length) is 1 mm. The electrode metal deposition rate is 0.2 Å/s. The microfluidic chip was fabricated from polydimethylsiloxane (PDMS), and was then integrated with the Gr-FETs, which was designed to work as both solution gate of Gr-FET and sensing action unit. The schematic diagram of Gr-FET integrated with microfluidic chip process is shown in Fig. 1a. The PDMS chip had fluidic channel of $10 \times 1$ mm$^2$ (length × width), which was aligned with the transduction channel of Gr-FETs. The detailed fabrication process is shown in Fig. S1. An Ag/AgCl reference electrode was used as gate electrode, which was placed in the outlet of microfluidic chip, and was connected to the transduction channel through the filled liquid. The electrical response of pH sensor to different seawater pH values was measured by using source meter (Keithley 2636B). The Dirac point shift of the Gr-FET-based pH sensor induced by the change of pH values is schematically shown in Fig. 1b. Figure 1b illustrates the working principle of Gr-FET pH

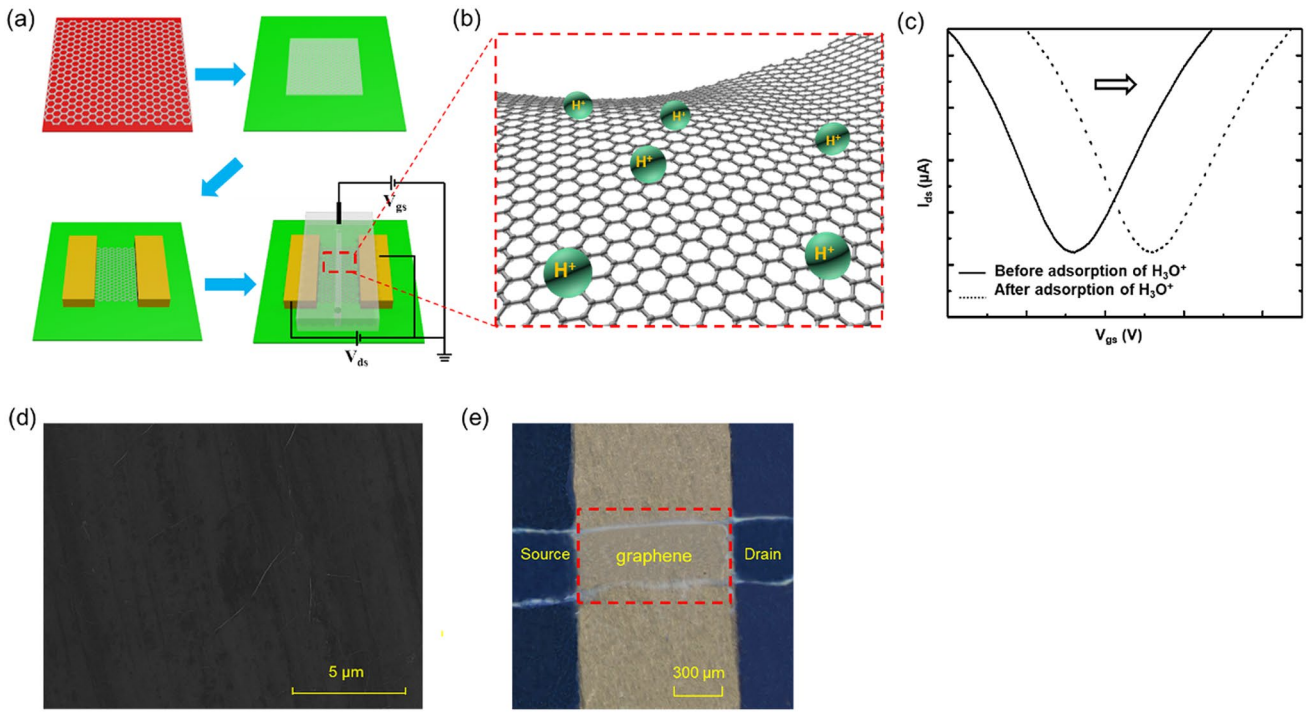


**Fig. 1** **a** Fabrication process and schematic diagram of Gr-FET-based pH sensor. **b** Illustration of pH detection by Gr-FET. **c** Response schematic of FET transfer characteristics to pH variation. **d** The SEM image of monolayer graphene. **e** Optical microscope image of Gr-FET

sensor. Defects on the edge of graphene can adsorb hydrons, which caused the shift of Dirac point, as shown in Fig. 1c. The SEM image of monolayer graphene was characterized by ZEISS Sigma500 with operating voltage of 15 kV and is shown in Fig. 1d. The SEM image shows that there are some micro-wrinkles formed during monolayer graphene transfer process (Fig. 1d). The optical image of transferred monolayer graphene on PI substrate shows clear connection between source and drain electrodes as shown in Fig. 1e).

## 3 Results and discussion

### 3.1 Characterization of monolayer graphene

The quality of monolayer graphene is crucial for transistor performance. Raman spectroscopy of the samples was conducted and the layers of graphene were recognized by the ratio of 2D peak over G peak, and Fig. 2a shows 2D/G ratio of 3.26, which indicates that the transferred graphene is monolayer with high quality. The reported thickness of monolayer graphene was ~ 0.4 nm [45]. Spatial Raman mapping of monolayer graphene over an area of $45 \times 25\ \mu m^2$ is shown in Fig. 2b. The spectrum of each point in the image was estimated by combining each reference spectrum of single-layer

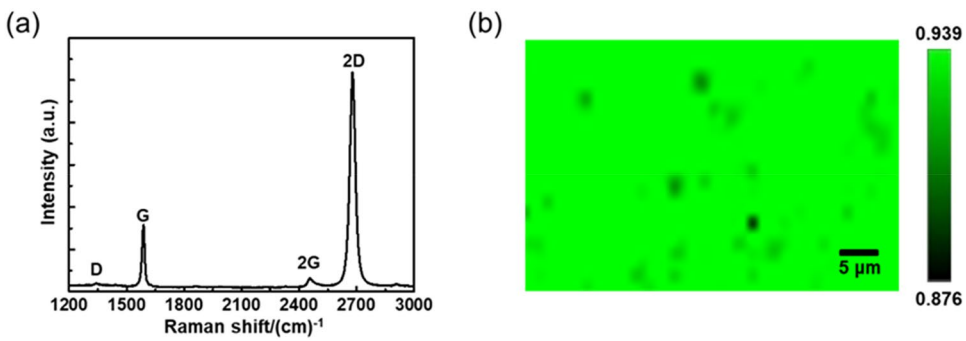


**Fig. 2** **a** Raman spectrum of transferred graphene with 2D/G of 3.26. **b** Raman mapping of monolayer graphene over an area of $45 \times 25\ \mu m^2$

graphene after scaling. The scale bar represents the similarity of single-layer graphene spectrum, which is more than 0.876 over the whole area. It is indicated that the transferred graphene has uniform properties.

### 3.2 Characterization of Gr-FET performance

After the integration of Gr-FET and microfluidic chip, the electrical characteristics were performed, which included the output and transfer characteristics. The typical output characteristics of Gr-FETs on polyimide (PI) and $Si/SiO_2$ substrates are shown in Fig. 3a and b. S/D voltage $V_{ds}$ was scanned from − 50 to 50 mV, and gate voltage $V_{gs}$ increased from − 0.1 to 0.3 V with a reference gate electrode (Ag/AgCl) in 1 × PBS solutions. The both devices show the linear relationship with $I_{ds}$–$V_{ds}$ at constant $V_{gs}$, and electronic transport can be modulated by $V_{gs}$. The source–drain current decreases with a slight reduction of the gate voltage, indicating that the device response is sensitive to the gate voltage [46]. And the typical transfer characteristics of Gr-FETs on both PI and $Si/SiO_2$ substrates are shown in Fig. 3c and d, which measured at the same conditions with fixed $V_{ds}$ = 50 mV and swiping $V_{gs}$ in 1 × PBS solutions. The ambipolar characteristics could be clearly observed at a small range of gate voltage under ambient conditions. The slight right shift of $V_{Dirac}$ (the gate voltage corresponding to the minimum conductance) suggests that graphene is p-doped by adsorbates in the environment [44, 47]. Compared with typical back-gate Gr-based FET, which is shown in Fig. S2, the solution-gated FETs show much better performance. The graphene FETs with solution gate showed a hole and electron mobility of 302 and 275 $cm^2/(V{\cdot}s)$, which was obtained based on transfer curve shown in Fig. S3. We conducted the electrical stability test of Gr-FET on PI substrates along with storage time after gate solution (1 × PBS) is loaded into channel. Transfer curves of the sensor on PI substrate present negligible change in 12 h as shown in Fig. S4, indicating the electrical performance of the sensor is very stable.

### 3.3 Gr-FET-based pH sensor characterizations

The sensing of a solution with different pH values is based on the graphene surface property change induced by $H^+$, which contributed to the shift of Dirac point in transfer characteristics of Gr-FET. To investigate the sensing performance of solution-gated Gr-FET pH sensor, 1 × PBS solution is used as gate solution, in which pH is adjusted to different values from 6 to 8. The transfer ($I_{ds} - V_{gs}$) curves of Gr-FET on both PI and $Si/SiO_2$ substrates with gate liquid solution are shown in Fig. 4a and b. The right shift of the $V_{Dirac}$ was obtained with the increase of pH values for both devices, indicating that $H_3O+$ ions induced the p-doping of the graphene [9]. The values of Dirac point were derived from transfer curve according to the given pH on both PI and $Si/SiO_2$ substrates, and show a linear relationship with pH values, as shown in Fig. 4c and d. Dirac point shift to higher value with pH value increase,

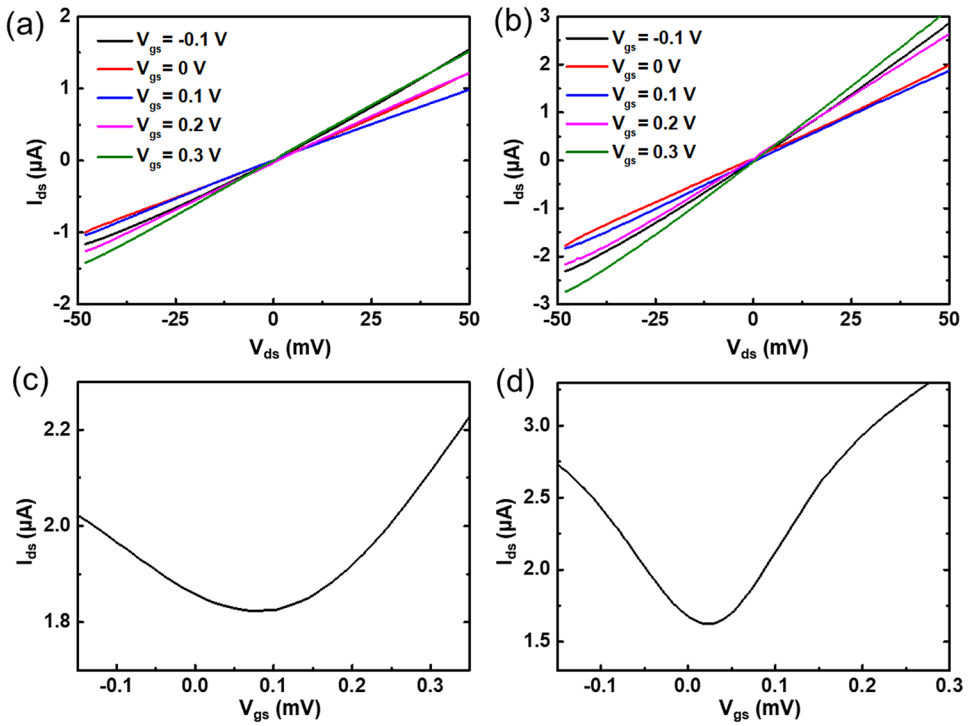


**Fig. 3** **a** Output characteristics of solution-gated Gr-FETs at various gate voltages on PI substrate. **b** Output characteristics of solution-gated graphene FETs at various gate voltages on $Si/SiO_2$ substrate. **c** Transfer characteristics of solution-gated graphene FET on PI substrate at drain–source bias $V_{ds}$ = 50 mV. **d** Transfer characteristics of solution-gated graphene FET on $Si/SiO_2$ substrate at drain–source bias $V_{ds}$ = 50 mV

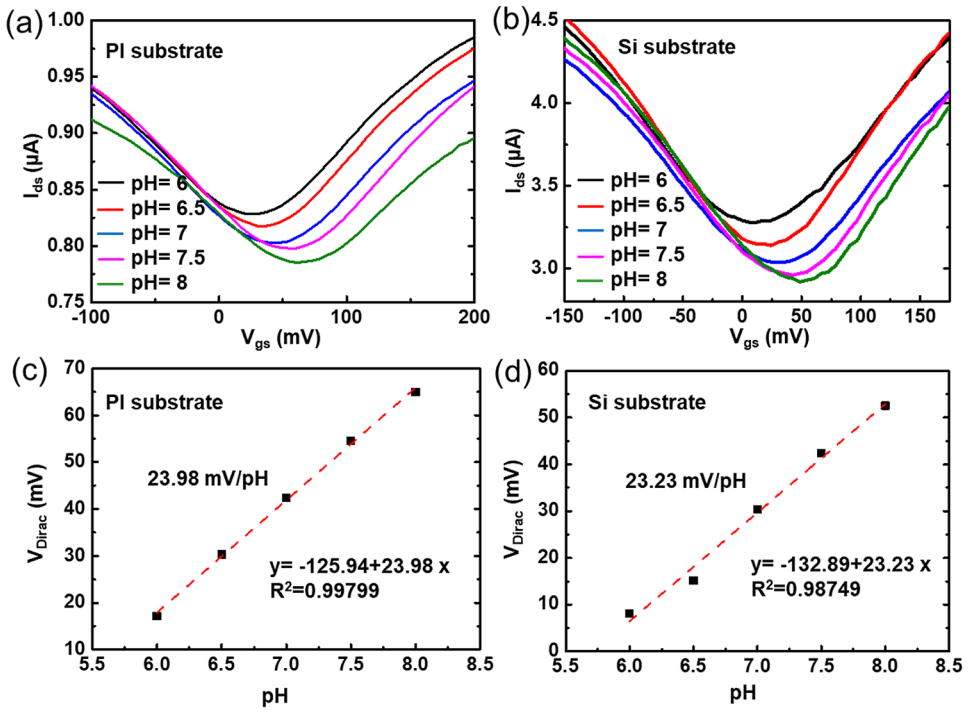


**Fig. 4** **a** $I_{ds} - V_{gs}$ curves of solution-gated Gr-based FETs operated in 1 × PBS buffer solutions with various pH values at $V_{ds}$ = 50 mV on PI substrate. **b** $I_{ds} - V_{gs}$ curve of solution-gated Gr-based FET operated in 1 × PBS buffer solution with various pH values at $V_{ds}$ = 50 mV on $Si/SiO_2$ substrate. **c** The linear relation between Dirac point $V_{Dirac}$ and pH value on PI substrate. **d** The linear relation between Dirac point $V_{Dirac}$ and pH value on $Si/SiO_2$ substrate

and the sensitivity of solution-gated Gr-FET is 23.98 and 23.23 mV/pH on both PI and $Si/SiO_2$ substrates. It indicated that the pH sensing performance of the Gr-based FET sensor on both flexible and $Si/SiO_2$ substrates is similar in 1 × PBS-based solution, which is consistent with the previous report [48].

The components in sample solution have important effects on the performance of pH sensor, and we conducted the pH sensing in seawater solution by adjusting pH values using HCl and NaOH. Transfer curves ($I_{ds}$–$V_{gs}$) of Gr-based FETs responding to seawater with different pH values on both PI and $Si/SiO_2$ substrates are shown in

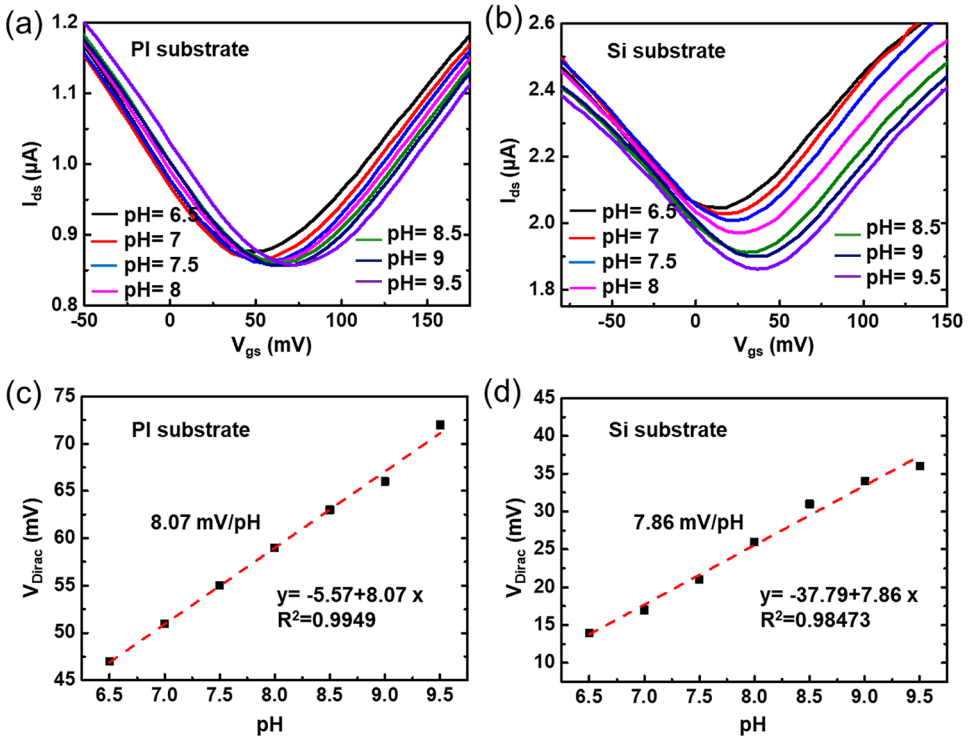


**Fig. 5** Transfer curves ($I_{ds} - V_{gs}$) of solution-gated Gr-based FETs pH sensors operated in seawater with various pH values at $V_{ds}$ = 50 mV **a** on PI and **b** on $Si/SiO_2$ substrate. The relationship between $V_{Dirac}$ and pH value **c** on PI substrate and **d** $Si/SiO_2$ substrate, respectively

Fig. 5a and b. The similar trend was observed for $V_{Dirac}$ in both devices. And they also shift to higher value when pH changes from low to high value in the range of 6.5–9.5. But a smaller shift value per pH in seawater solution was obtained compared to that in 1 × PBS solution. Figure 5c and d shows the values of Dirac point dependence on pH values in seawater from Gr-FET on PI and $Si/SiO_2$ substrates. It also shows linear relationship between Dirac point and pH values in both devices with spiked seawater solution. Gr-based FET pH sensors present the sensitivity of 8.07 mV/pH on PI substrates and 7.86 mV/pH on $Si/SiO_2$ substrates. To confirm the tested results in seawater solution, we performed another 4 more tests. The sensitivity results were obtained from 4 different tests as shown in Figs. S5 and S6, and the average sensitivity values of the sensors are 7.82 mV/pH on PI substrates and 7.53 mV/pH on $Si/SiO_2$ substrates. It confirmed that the pH sensitivity of the devices tested in seawater is much lower than that tested in 1 × PBS solution. As reported previously, the ion type and ion strength of the solution have huge effect on the Gr-based FET pH sensor performance [20, 49]. The $V_{Dirac}$ shift was more sensitive to the concentration of $Na^+$ than to the concentrations of $Cl^-$ or $K^+$[49]. At high ionic strength, the double-layer capacitance at the graphene-buffer interface increases and the surface potential decreases [20]. By comparison, the concentration of $Na^+$ in 1 × PBS was 157 mM, more than 300 times higher than that in seawater (only 0.473 mM). Also there are some other ions in the seawater (Table S1). Therefore, the different ion type and concentration in the solution could be contributed to the sensitivity reduction of the devices in seawater [38, 39].

The stability of pH sensor is one of the most important parameters in practical applications. Here, we performed pH test cycles using seawater solution. The cycled pH test results are shown in Fig. 6a and b for the devices on PI and $Si/SiO_2$ substrates. Gr-based FET pH sensor detects the pH value in seawater from 6.5 to 9.5 with step of 0.5, and then from 9.5 down to 6.5. During the measurements, the $V_{gs}$ was swept from − 100 to 200 mV at a $V_{ds}$ of 50 mV. Each solution was tested 5 times in succession, and the average sensitivity is shown in Fig. 6a and b. The Gr-based FET pH sensor on PI substrate shows clear transition curve with pH value change, while large fluctuation appeared for the sensor on $Si/SiO_2$ substrate. It indicated that the Gr-based FET pH sensor on PI substrate shows better stability than that on $Si/SiO_2$ substrate, which may be due to the effect of charged impurities trapped on the $SiO_2$ substrate [44, 47]. In order to more accurately compare the sensor's sensitivity stability, the relationship between $V_{Dirac}$ and pH value (c) of each cycle was plotted for the sensors on PI substrate and (d) $Si/SiO_2$ substrates. The results are shown in Fig. 6c and d which are similar to Fig. 6a and b. It further confirmed that the Gr-based FET pH sensor on PI substrate presented slightly better stability than that on $Si/SiO_2$ substrate.

One of the advantages of graphene is its mechanical properties, which can be applied in the field of flexible electronics. The transfer characteristics of Gr-FET were

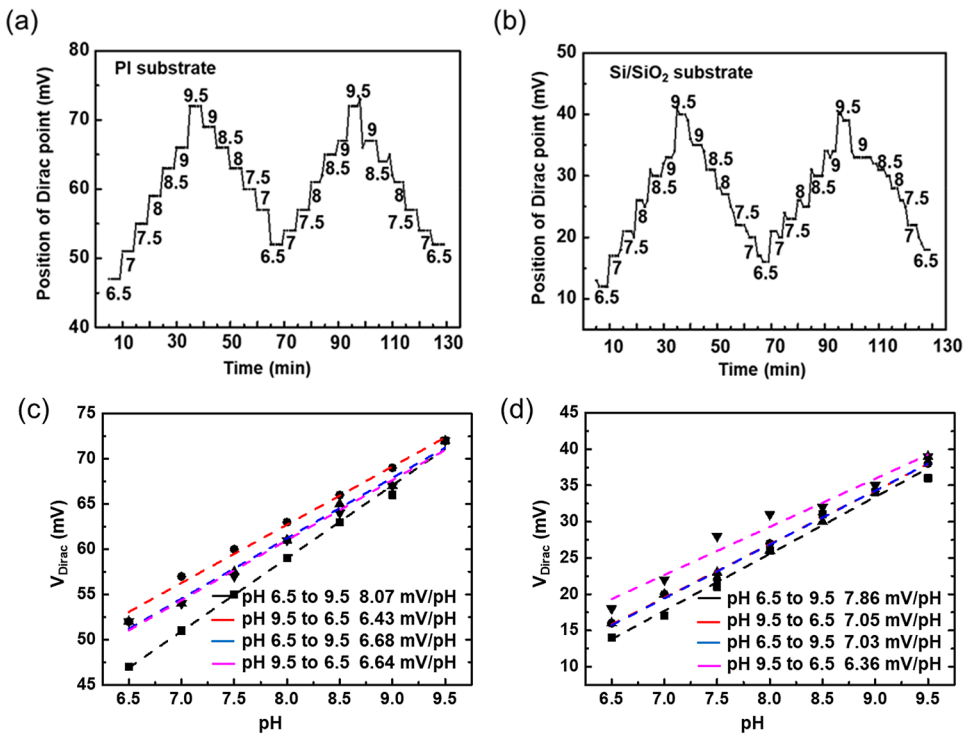


**Fig. 6** Cycled pH detection of Gr-based FET **a** on PI and **b** $Si/SiO_2$ substrates. Cycled pH sensitivity of Gr-based FET **c** on PI and **d** $Si/SiO_2$ substrates, respectively

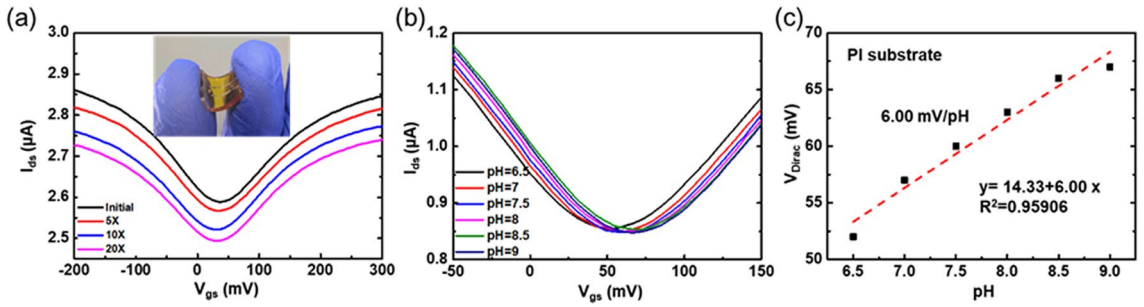


**Fig. 7** **a** Transfer curves of a flexible Gr-FET over multiple bending cycles. Inset shows the optical image of pH sensor under bending. **b** Transfer characteristics after bent Gr-FET pH sensor with different pH values. **c** The linear relation between Dirac point $V_{Dirac}$ and pH value after bending

tested before and after bending, as shown in Fig. 7a, and the optical image of pH sensor under bending is shown in the inset of Fig. 7a. As the bending period increases, the Dirac point shifts to left slightly. The slope of the transfer curve decreases, indicating the decrease of both electron and hole mobility because of the bending-induced stress. However, the shift caused by bending does not affect the accuracy of pH sensing, because the Dirac point response to test sample can be referred to the Dirac value after bending. As shown in Fig. 7b and c, after 20 times mechanical bends with radius of 12 mm, response of $V_{Dirac}$ to pH was almost similar to that before bending, and sensitivity of the sensor degraded slightly to 6.00 mV/pH, which may be due to the bending-induced stress leading to the performance decrease of the device.

Most importantly, we conducted the real seawater detection using our Gr-based FET pH sensor. The Gr-based FET pH sensor on PI substrate was selected to test the pH of seawater samples because it showed better stability as presented above. Seawater samples were collected from the off-shore near Shandong University (Tsingtao) campus in Jiaozhou Bay every day from 14 to 20 June, 2019, and each sample was tested for 6 times using our Gr-based FET pH sensor and commercialized pH meter (OHAUS ST3100). The transfer characteristics of Gr-based FET pH sensor responding to seawater samples for seven

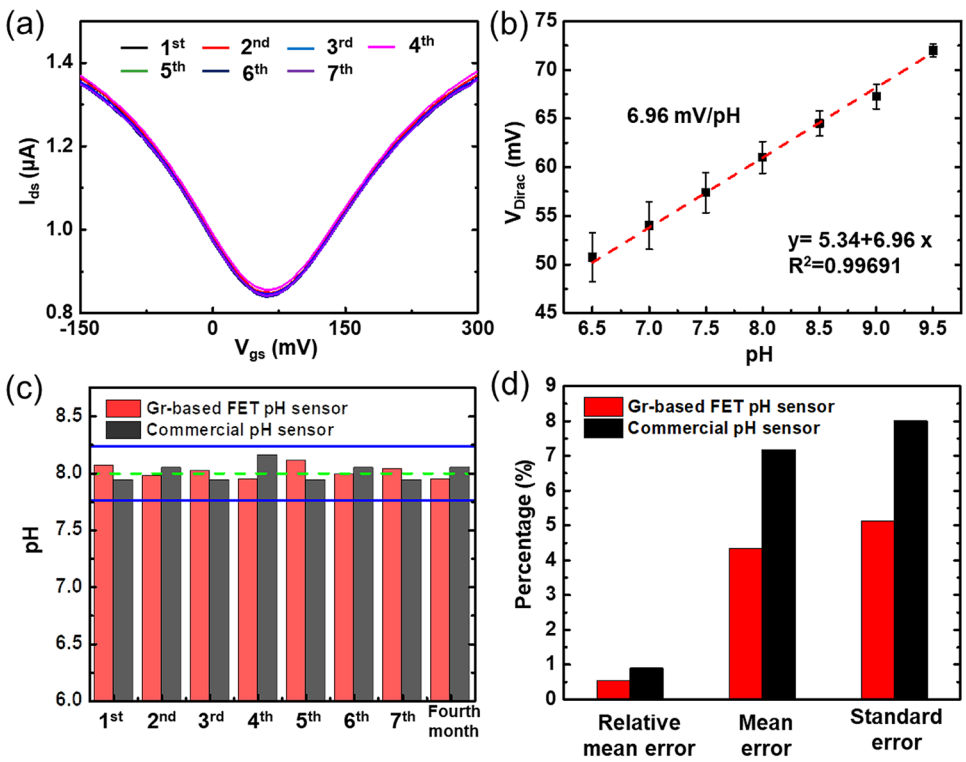


**Fig. 8** **a** The transfer curves of Gr-based FET pH sensor on PI substrate by testing real seawater from the off-shore near Shandong University (Tsingtao) campus in Jiaozhou Bay every day from 14 to 20 June, 2019. **b** Mean pH sensitivity value of the Gr-based FET seawater pH sensors on PI substrate in seawater solution. Comparison of the seawater pH measurement results **c** (Green dash line represents mean pH value measured by commercial pH meter, and blue lines represent 3% variation relative measured mean pH values by commercial pH meter) and **d** the measured datum error analyzation between Gr-based FET pH sensor and the commercialized pH meter

consecutive days are shown in Fig. 8a, which shows very stable transfer curves. According to the linear relationship between Dirac point and pH value as shown in Fig. 8b, the pH values of seawater samples are derived, and are shown in Fig. 8c. Detailed test values from our Gr-based FET pH sensor and the commercialized pH meter are listed in Fig. S7 and Table S2. The average pH value of the samples is 8.023 and 8.003 detected by our Gr-based FET pH sensor and commercialized pH meter (OHAUS ST3100), respectively. The less than 3% of relative error was obtained. The measured datum error analyzation results showed that the performance of the Gr-based FET pH sensor is better than that of commercialized pH meter (Fig. 8d). To further test the stability of the sensor, we performed the pH detection of seawater after the sensor was stored 4 months in a 4 °C refrigerator. The pH value of the seawater measured by the pH sensor and commercial pH meter is 7.95 and 8.05. The error of the pH test result is still within 3%, as shown in Fig. 8c. It indicates that the Gr-based FET pH sensor has potential to be the next-generation portable, stable and real-time pH detection devices in the future.

## 4 Conclusion

In summary, we demonstrated a Gr-FET-based flexible pH sensor, which was integrated with a microfluidic chip to conduct fast and sensitive pH value detection of the seawater. The sensor realized real seawater pH detection in 1 min with a sensitivity of 8.07 mV/pH. Real-time seawater pH detection results show very stable performance with less than 3% of relative error. The integrated chip is compact and portable, which is favorable to set up portable and minimized equipment. More importantly, the pH sensor is based on the electrical response to graphene surface property change, and is free from the influence of vibration during test, which is especially important on scientific research ship during marine survey.

**Acknowledgements** This work was supported by the National Key R&D Plan of China (Grant No. 2019YFC1407800), Natural Science Foundation for Distinguished Young Scientist of Shandong Province (Grant No. JQ201814), the Key Research Plan of Shandong Province (2017GGX10106) and Collaborative Innovation Center of Technology and Equipment for Biological Diagnosis and Therapy in Universities of Shandong. We would like to thank Haiyan Yu, Xiaomin Zhao, Sen Wang and Yuyu Guo from State Key laboratory of Microbial Technology of Shandong University for help and guidance in material characterization.

**Author contributions** YZ and LH designed the study; JG carried out the experiments and wrote this manuscript; YW assisted in the completion of the experiment; YH conducted graphene nanosheets characterization; YG and CW made microfluidic chips.

## Compliance with ethical standards

**Conflict of interest** All the authors declare no conflicts of interest with this work.

## References

1. K.S. Novoselov, A.K. Geim, S.V. Morozov et al., Nature **438**, 197 (2005). https://doi.org/10.1038/nature04233
2. Y. Zhang, Y.W. Tan, H.L. Stormer, P. Kim, Nature **438**, 201 (2005). https://doi.org/10.1038/nature04235
3. K.S. Kim, Y. Zhao, H. Jang et al., Nature **457**, 706 (2009). https://doi.org/10.1038/nature07719
4. W. Han, D. Nezich, K. Jing, T. Palacios, IEEE Electron Device Lett. **30**, 547 (2009). https://doi.org/10.1109/LED.2009.2016443
5. H. Wang, A. Hsu, J. Wu, J. Kong, T. Palacios, IEEE Electron Device Lett. **31**, 906 (2010). https://doi.org/10.1109/LED.2010.2052017
6. X. Wang, L. Zhi, K. Müllen, Nano Lett. **8**, 323 (2008). https://doi.org/10.1021/nl072838r
7. V.P. Verma, S. Das, I. Lahiri et al., Appl. Phys. Lett. **96**, 203108 (2010). https://doi.org/10.1063/1.3431630
8. S. Bae, H. Kim, Y. Lee et al., Nat. Nanotechnol. **5**, 574 (2010). https://doi.org/10.1038/nnano.2010.132
9. P.K. Ang, W. Chen, A.T.S. Wee, K.P. Loh, J. Am. Chem. Soc. **130**, 14392 (2008). https://doi.org/10.1021/ja805090z
10. S.K. Lee, H.Y. Jang, S. Jang et al., Nano Lett. **12**, 3472 (2012). https://doi.org/10.1021/nl300948c
11. C.-C. Lu, Y.-C. Lin, C.-H. Yeh, J.-C. Huang, P.-W. Chiu, ACS Nano **6**, 4469 (2012). https://doi.org/10.1021/nn301199j
12. Q. He, S. Wu, S. Gao et al., ACS Nano **5**, 5038 (2011). https://doi.org/10.1021/nn201118c
13. F. Schwierz, Nat. Nanotechnol. **5**, 487 (2010). https://doi.org/10.1038/nnano.2010.89
14. Y. Shao, J. Wang, H. Wu, J. Liu, I.A. Aksay, Y. Lin, Electroanalysis **22**, 1027 (2010). https://doi.org/10.1002/elan.200900571
15. Y. Dan, Y. Lu, N.J. Kybert, Z. Luo, A.C. Johnson, Nano Lett. **9**, 1472 (2009). https://doi.org/10.1021/nl8033637
16. C. Berger, Z. Song, X. Li et al., Science **312**, 1191 (2006). https://doi.org/10.1126/science.1125925
17. L. Lin, Y. Liu, L. Tang, J. Li, Analyst **136**, 4732 (2011). https://doi.org/10.1039/C1AN15610A
18. Q. He, S. Wu, Z. Yin et al., Chem. Sci. **3**, 1764 (2012). https://doi.org/10.1021/jp201667p
19. Y. Ohno, K. Maehashi, Y. Yamashiro, K. Matsumoto, Nano Lett. **9**, 3318 (2009). https://doi.org/10.1021/nl901596m
20. I. Heller, S. Chatoor, J. Männik, M.A. Zevenbergen, C. Dekker, S.G. Lemay, J. Am. Chem. Soc. **132**, 17149 (2010). https://doi.org/10.1021/ja104850n
21. S. Karastogianni, S. Girousi, S. Sotiropoulos, Encycl. Food Health (2016). https://doi.org/10.1016/B978-0-12-384947-2.00538-9
22. P. Salvo, B. Melai, N. Calisi et al., Sens. Actuators B **256**, 976 (2018). https://doi.org/10.1016/j.snb.2017.10.037
23. P. Kraikaew, S. Jeanneret, Y. Soda et al., ACS Sensors **5**, 650 (2020). https://doi.org/10.1021/acssensors.0c00031
24. R. Pfattner, A.M. Foudeh, S. Chen et al., Adv. Electron. Mater. **5**, 1800381 (2019). https://doi.org/10.1002/aelm.201800381
25. K. Zhou, Z. Zhao, P. Yu, Z. Wang, Sens. Actuators B **320**, 128403 (2020). https://doi.org/10.1016/j.snb.2020.128403
26. S. Falina, M. Syamsul, Y. Iyama, M. Hasegawa, Y. Koga, H. Kawarada, Diam. Relat. Mater. **91**, 15 (2019). https://doi.org/10.1016/j.diamond.2018.11.005

27. N. Poma, F. Vivaldi, A. Bonini et al., Microchem. J. **148**, 248 (2019). https://doi.org/10.1016/j.microc.2019.05.001
28. J. Ristein, W. Zhang, F. Speck et al., J. Phys. D (2010). https://doi.org/10.1088/0022-3727/43/34/345303
29. X. Tan, H.-J. Chuang, M.-W. Lin, Z. Zhou, M.M.-C. Cheng, J. Phys. Chem. C **117**, 27155 (2013). https://doi.org/10.1021/jp409116r
30. S.S. Kwon, J. Yi, W.W. Lee et al., ACS Appl. Mater. Interfaces **8**, 834 (2016). https://doi.org/10.1021/acsami.5b10183
31. Z. Wang, K. Yi, Q. Lin et al., Nat. Commun. **10**, 1544 (2019). https://doi.org/10.1038/s41467-019-09573-4
32. W. Wei, Z. Zeng, W. Liao, W.K. Chim, C. Zhu, ACS Appl. Nano Mater. **3**, 403 (2020). https://doi.org/10.1021/acsanm.9b02037
33. C. Staudinger, M. Strobl, J. Breininger, I. Klimant, S.M. Borisov, Sens. Actuators B **282**, 204 (2019). https://doi.org/10.1016/j.snb.2018.11.048
34. K. Xu, Y. Kitazumi, K. Kano, O. Shirai, Electrochem. Commun. **101**, 73 (2019). https://doi.org/10.1016/j.elecom.2019.03.003
35. T. Mitsuno, Y. Taniguchi, Y. Ohno, M. Nagase, Appl. Phys. Lett. **111**, 213103 (2017). https://doi.org/10.1063/1.4994253
36. T. Ono, Y. Kanai, K. Inoue et al., Nano Lett. **19**, 4004 (2019). https://doi.org/10.1021/acs.nanolett.9b01335
37. X Liu, T Du, H Zhang, C Sun (2019) 2019 41st Ann. Int. Conf. IEEE Eng. Med. Biol. Soc. (EMBC), https://doi.org/10.1109/EMBC.2019.8856991
38. T.-Y. Chen, P.T.K. Loan, C.-L. Hsu et al., Biosens. Bioelectron. **41**, 103 (2013). https://doi.org/10.1016/j.bios.2012.07.059
39. M.J. Kiani, M.T. Ahmadi, H.K. Feiz Abadi, M. Rahmani, A. Hashim, F.K. Che Harun, Nanoscale Res. Lett. **8**, 173 (2013). https://doi.org/10.1186/1556-276X-8-173
40. B. Anes, R.J.N. Bettencourt, C. da Silva, M.F.C. Oliveira, Talanta **193**, 118 (2019). https://doi.org/10.1016/j.talanta.2018.09.075
41. J.W. Runcie, C. Krause, S.A. Torres Gabarda et al., Biogeosciences **15**, 4291 (2018). https://doi.org/10.5194/bg-15-4291-2018
42. K. McLaughlin, A. Dickson, S.B. Weisberg et al., Reg. Stud. Mar. Sci. **12**, 11 (2017). https://doi.org/10.1016/j.rsma.2017.02.008
43. V.C. Pinto, C.F. Araújo, P.J. Sousa, L.M. Gonçalves, G. Minas, Sens. Actuators B **290**, 285 (2019). https://doi.org/10.1016/j.snb.2019.03.098
44. I. Jung, D.A. Dikin, R.D. Piner, R.S. Ruoff, Nano Lett. **8**, 4283 (2008). https://doi.org/10.1021/nl8019938
45. M.H. Rümmeli, S. Gorantla, A. Bachmatiuk, et al. Chem. Mater. **25**, 4861 (2013). https://doi.org/10.1021/cm401669k
46. J. Chang, S. Mao, Y. Zhang et al., Nanoscale **5**, 3620 (2013). https://doi.org/10.1039/C3NR00141E
47. X. Wang, X. Li, L. Zhang et al., Science **324**, 768 (2009). https://doi.org/10.1126/science.1170335
48. B. Mailly-Giacchetti, A. Hsu, H. Wang et al., J. Appl. Phys. **114**, 084505 (2013). https://doi.org/10.1063/1.4819219
49. M.H. Lee, B.J. Kim, K.H. Lee et al., Nanoscale **7**, 7540 (2015). https://doi.org/10.1039/C5NR00414D


**Publisher's Note** Springer Nature remains neutral with regard to jurisdictional claims in published maps and institutional affiliations.